GEOPHYSICAL RESEARCH LETTERS, VOL. 35, L13602, doi:10.1029/2008GL033856, 2008

Rapid generation of high-frequency internal waves beneath a wind and wave forced oceanic surface mixed layer

Jeff A. Polton,[1,2] Jerome A. Smith,[1] J. A. MacKinnon,[1] and Andrés E. Tejada-Martínez[3]

Received 7 March 2008; revised 9 May 2008; accepted 2 June 2008; published 8 July 2008.

[1] High-frequency internal waves generated by Langmuir motions over stratified water may be an important source of turbulent mixing below the surface mixed layer. Large eddy simulations of a developing mixed layer and inertial current are employed to investigate this phenomena. Uniform surface wind stress and parallel Stokes drift wave forcing rapidly establishes a turbulent mixed-layer flow, which (as the inertial motion veers off the wind) generates high-frequency internal waves in the stratified fluid below. The internal waves evolve such that their vector phase velocity matches the depth-averaged mixed-layer velocity that rotates as an inertial oscillation. The internal waves drain energy and momentum from the mixed layer on decay time-scales that are comparable to those of near-inertial oscillations. The high-frequency waves, which are likely to be trapped in the transition layer, may significantly contribute to mixing there and thus provide a potentially important energy sink for mixed-layer inertial motions.
Citation: Polton, J. A., J. A. Smith, J. A. MacKinnon, and A. E. Tejada-Martínez (2008), Rapid generation of high-frequency internal waves beneath a wind and wave forced oceanic surface mixed layer, *Geophys. Res. Lett.*, *35*, L13602, doi:10.1029/2008GL033856.

1. Introduction

[2] Langmuir processes associated with the interaction between surface waves and wind driven currents very near the surface of the ocean augment the mixing of the surface layer, and can help maintain the mixed state against re-stratification [*O'Brien et al.*, 1991; *Li and Garrett*, 1997; *Gargett et al.*, 2004]. Observational evidence shows that turbulent mixing extends well below what can be explained by direct entrainment by mixed-layer currents [*Rippeth et al.*, 2005; T. M. S. Johnston and D. L. Rudnick, Observations of the transition layer, submitted to *Journal of Physical Oceanography*, 2008, and references therein].

[3] Traditionally a downward energy flux associated with near-inertial oscillations has been identified as responsible for this sub-mixed-layer mixing [*Bell*, 1978]. However, analyses of the Ocean Storms experiment showed that downward near-inertial flux was not sufficient to explain the observed decrease in surface mixed-layer energy [*D'Asaro et al.*, 1995]. In this study we show that, even under weak wind and wave forcing, high-frequency internal waves can be generated by Langmuir circulations that form rapidly, penetrate to the bottom of the mixed layer, and interact with the stratification [cf. *Chini and Leibovich*, 2005]. Since the stratification decreases below the transition layer, these waves are trapped and must deposit their energy there, contributing to the mixing processes. While the details differ, the mechanism in general resembles one first suggested by *Bell* [1978], and a similar one identified for equatorial internal wave radiation by *Wijesekera and Dillon* [1991]. One key difference is that, while Bell posited a broad range of internal waves being generated, both *Wijesekera and Dillon*'s [1991] observations and our numerical simulation results show a relatively narrow band of high-frequency internal waves very close to the buoyancy frequency, N.

[4] This letter is structured as follows. The model setup and parameters are detailed in section 2, results and analyses in section 3. A summary is given in section 4.

2. Model Details

[5] Three dimensional turbulent dynamics of the ocean mixed layer over stratified regions are modeled using a large eddy simulation (hereafter LES) technique where the model has sufficient temporal and spatial resolution to capture the large-scale turbulent motions. To constrain the problem we restrict our interest to the interactions on the flow by representing the effect of surface waves as a prescribed Stokes drift velocity,

$$u_s = U_s e^{z/\delta_s} \tag{1}$$

where U_s is the Stokes drift at the surface and $\delta_s = 1/2k$ is the Stokes depth scale for a monochromatic surface wave with wavenumber k [*Phillips*, 1977]. While this suppresses any feedback on the waves, this is justified for the waves and current scales of interest [*Craik and Leibovich*, 1976; *Phillips*, 2001].

[6] Previous computational studies of turbulent boundary layers have employed LES techniques for the atmosphere [*Mason and Thompson*, 1992; *Coleman*, 1999] as well as in the ocean [*Zikanov et al.*, 2003]. Following *Skyllingstad and Denbo* [1995] and *McWilliams et al.* [1997] we perform LES of the wave-filtered Craik-Leibovich (C-L) equations [*Craik and Leibovich*, 1976]. The C-L equations are a version of the Navier-Stokes equations that have been averaged over many surface wave cycles and represent the

[1] Scripps Institution of Oceanography, University of California, San Diego, La Jolla, California, USA.
[2] Now at Proudman Oceanographic Laboratory, Liverpool, UK.
[3] Civil and Environmental Engineering, University of South Florida, Tampa, Florida, USA.

0094-8276/08/2008GL033856$05.00

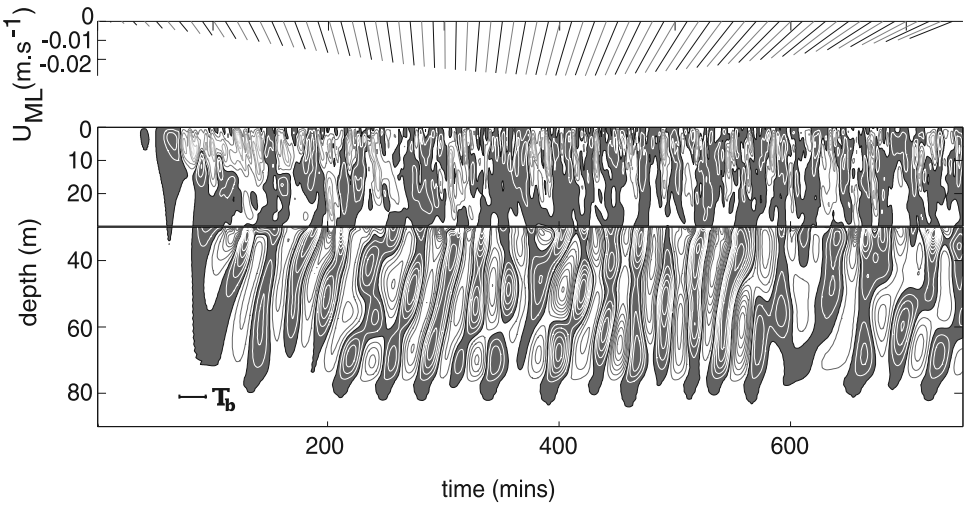

Figure 1. Contours of w/u_* as a function of depth and time. Simulation initially has a 30 m deep well mixed upper layer (contour interval of 1) on top of layer of constant stratification (contour interval of 0.1). Black denotes downwelling velocities. The stick plot shows the evolution of the horizontally and depth averaged mixed-layer velocity. Sloping bands in the stratified layer signal the presence of downward propagating internal waves. The buoyancy period, $T_b = 2\pi/N$, is illustrated on the figure.

net effect of the waves in terms of the Stokes drift. These equations are:

$$\frac{D\boldsymbol{u}}{Dt} + \boldsymbol{f} \times (\boldsymbol{u} + \boldsymbol{u_s}) = -\nabla\pi - \frac{g\rho'}{\rho_0}\hat{\mathbf{z}} + \boldsymbol{u_s} \times \boldsymbol{\omega} + SGS, \quad (2)$$

$$\nabla \cdot \boldsymbol{u} = 0, \quad (3)$$

$$\frac{D\theta}{Dt} + \boldsymbol{u_s} \cdot \nabla\theta = SGS. \quad (4)$$

Here $\boldsymbol{u} = (u, v, w)$ is the three dimensional wave-averaged Eulerian velocity, $\boldsymbol{f} = f\hat{\mathbf{z}}$ is the Coriolis parameter, $\hat{\mathbf{z}}$ is the upward unit vector, $\boldsymbol{\omega} = \nabla \times \boldsymbol{u}$ is the local vorticity vector, $D/Dt = \partial/\partial t + \boldsymbol{u} \cdot \nabla$ is the material derivative and the equation of state is a simple function of temperature, $\rho'/\rho_0 = -\theta'/\theta_0$, where $\theta_0 = 288.17\ K$ and $\rho_0 = 1000$ kg m^{-3}. The generalized pressure, π, given by

$$\pi = \frac{p}{\rho_0} + \frac{1}{2}\boldsymbol{u_s}^2 + \boldsymbol{u} \cdot \boldsymbol{u_s}. \quad (5)$$

The domain is horizontally periodic with 48 grid points in each direction spanning its width $L = 225$ m. In the vertical direction 128 grid points are smoothly stretched over the domain of depth $H = 90$ m with the minimum spacing at the surface, $\Delta z_0 = 0.2812$ m, and the maximum at the bottom, $\Delta z_H = 1.0524$ m. The subgrid scale processes (denoted as SGS) are parameterized using a first order Smagorinsky closure model based on similarity theory at the surface [*Lewis*, 2005], such that the mixing length, L_m, is given by $L_m^{-2} = (C_0\Delta)^{-2} + (\kappa(|z| + \Delta z_0))^{-2}$, where $\kappa = 0.4$, $C_0 = 0.16$ and $\Delta = (\Delta x^2 \Delta z)^{1/3}$. A discussion of this model including the coefficient C_0 is given by *Mason and Thompson* [1992] and is reviewed by *Porté-Agel et al.* [2000]. A sponge layer is employed in the lowest 15 m, which relaxes the vertical velocity back to the instantaneous horizontal average, to prevent wave reflection. A wind stress is applied to the surface layer using an imposed friction velocity u_*, and a small destabilizing heat flux, -5 Wm^{-2}, is applied to the surface to help trigger motions [*Lewis*, 2005]. The simulations are initialized from rest with a continuous density field that is constant in the upper 30 m and constantly stratified below with $N = 4.4 \times 10^{-3}$ s^{-1}. In the simulation presented here, the following parameter values were chosen: $f = 10^{-4}$ s^{-1}, $u_* = 6.1 \times 10^{-3}$ ms^{-1}, $U_s = 0.068$ ms^{-1}, $k = 0.105$ m^{-1}. Both wind stress and Stokes drift were steady and positive in the x-direction.

[7] The numerical method solving the governing equations employs a hybrid pseudo-spectral/finite-difference discretization. Downwind and crosswind directions are discretized spectrally via Fourier series and the vertical direction is discretized with high order compact finite-difference schemes [*Lele*, 1992] allowing for grid-stretching in that direction. Time-marching consists of a second order time-accurate pressure correction scheme on a non-staggered grid analyzed by *Armfield and Street* [2000]. Further details of the method and validation studies can be found in work by *Tejada-Martínez and Grosch* [2007] and A. E. Tejada-Martínez et al. (A non-hydrostatic large-eddy simulator of turbulence, manuscript in preparation, 2008).

3. Results

[8] We define $\boldsymbol{U_{ML}}$ as the depth and horizontally averaged mixed-layer velocity. Figure 1 shows the vertical velocity at a x-y point location as a function of depth and time with $\boldsymbol{U_{ML}}$ plotted as vector sticks above. The mixed-layer velocity is characterized by a steady wind-driven southward velocity with a superimposed inertial oscillation. Contours of w/u_* are plotted with split plots. The upper 30 m plot, which includes the mixed layer, has a contour interval of w/u_* and is clearly distinct from the stratified region below, where the interval is increased by a factor of 10. In

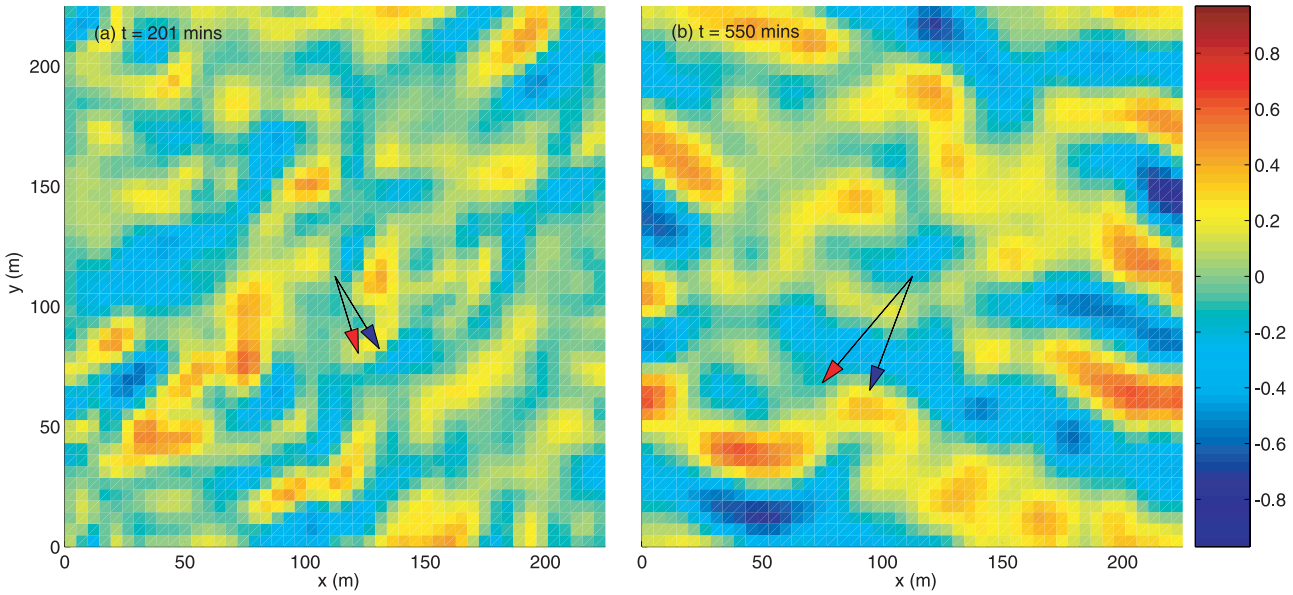

Figure 2. Plots show snap shots of w/u_* in the stratified layer after (a) 201 minutes ($U_{ML} = 0.018$ ms^{-1}) and (b) 550 minutes ($U_{ML} = 0.031$ ms^{-1}). The red and blue arrows show the relative magnitude and direction of $\boldsymbol{U_{ML}}$ and $\boldsymbol{c_p}$ respectively.

the upper plot the Langmuir turbulence manifests as alternating upwelling and downwelling that penetrates throughout the mixed layer. However, when the mixed-layer velocity diminishes the strength of w/u_* also diminishes. Beneath the mixed layer, forward tilting bands of upwelling and downwelling that characterize downward propagating energy are found. These internal waves have different periods to the mixed-layer processes but, as we show, the wave parameters are instead controlled by the mixed layer. The onset of the Langmuir cells and internal waves is rapid, consistent with observations [*Langmuir*, 1938; *Faller*, 1971; *Leibovich*, 1983; *Thorpe*, 2004].

[9] In order to visualize the four dimensional flow field that are inhomogeneous in depth and time we difference horizontal FFTs of w in either depth or time in order to extract the vertical wavenumber or the frequency of the field. For example, to extract the frequency define

$$F(\boldsymbol{k_h}, z, t) = \frac{1}{2\pi} \int \int w(\boldsymbol{x}, z, t) e^{-i\boldsymbol{k_h}\cdot\boldsymbol{x}} dx\, dy, \tag{6}$$

where the three dimensional wavenumber is given by (k_x, k_y, k_z) = ($\boldsymbol{k_h}$, k_z). Then the time-staggered complex power, $P_{\Delta t}(\boldsymbol{k_h}, z, t) = F(\boldsymbol{k_h}, z, t)\, F^*(\boldsymbol{k_h}, z, t + \Delta t)$, which is constructed from F and its complex conjugate, is such that its complex phase angle, $\omega\Delta t$, gives the frequency $\omega(\boldsymbol{k_h}, z, t)$ for a known time step Δt. Similarly, vertical wavenumber k_z can be extracted by constructing a power $P_{\Delta z}$ from vertically staggered F.

[10] The horizontal phase velocity, $\boldsymbol{c_p}$, of the waves is then computed as the inverse of the power-weighted 'slowness'. Averaging slowness preserves the mean wavenumber for a superposition of vector waves,

$$\boldsymbol{c_p}(z,t) = \left\{ \overline{|P_{\Delta t}(\boldsymbol{k_h}, z, t)| \frac{\boldsymbol{k_h}}{\omega(\boldsymbol{k_h}, z, t)}}^{\boldsymbol{k_h}} \right\}^{-1}. \tag{7}$$

In computing the phase speed the components $P_{\Delta t}$ and ω are first averaged over a 60 minute moving window to smooth the data and the averaging (overbar) is computed in $\boldsymbol{k_h}$-space.

[11] The horizontal rotation of the internal wave propagation is shown in Figure 2. Two snap shots show w (shaded) at 50 m depth after 201 and 550 minutes (plots *a* and *b* respectively). The blue arrow shows the corresponding direction of $\boldsymbol{c_p}$ and the red arrow shows the direction and relative magnitude of $\boldsymbol{U_{ML}}$ projected from the mixed layer above. Figure 2 shows $\boldsymbol{c_p}$ lagging $\boldsymbol{U_{ML}}$ as the mixed-layer mean flow and $\boldsymbol{k_h}$ rotate with time.

[12] Figure 3 emphasizes the association between $\boldsymbol{U_{ML}}$ and $\boldsymbol{c_p}$. The top plot shows details of $\boldsymbol{U_{ML}}$ in the 30 m mixed layer and the lower plot shows $\boldsymbol{c_p}$ from 30–90 m. The magnitudes are shaded and the directions (relative to the positive x-direction) are contoured in degrees. Hence there is a constraint on the internal waves that, for some phase lag ϕ, the phase velocity lags the mixed-layer average velocity and is given by:

$$\boldsymbol{c_p} \approx e^{i\phi} \boldsymbol{U_{ML}}. \tag{8}$$

[13] For internal waves that satisfy the dispersion relationship, it remains to identify one more constraint to uniquely determine the internal wave parameters, $\boldsymbol{k_h}$, k_z, ω as a function of the large scale parameters: buoyancy frequency N, mixed-layer depth H_0, and $\boldsymbol{U_{ML}}$. One might expect that the horizontal wavenumber at the base of the mixed layer would reflect the size of the Langmuir cell above, varying inversely with the depth of the mixed layer. Hence four additional simulations, R1–R4, are constructed to test the hypothesis that $k_h H_0 \approx n\pi/2$ (n = 1,2) and are detailed in Table 1. Simulations R1–R4 are computed on a smaller horizontal grid (L = 150 m) that preserves the grid spacing. Otherwise R0 and R1 are identical. This verifies that the simulated horizontal wavenumbers are not deter-

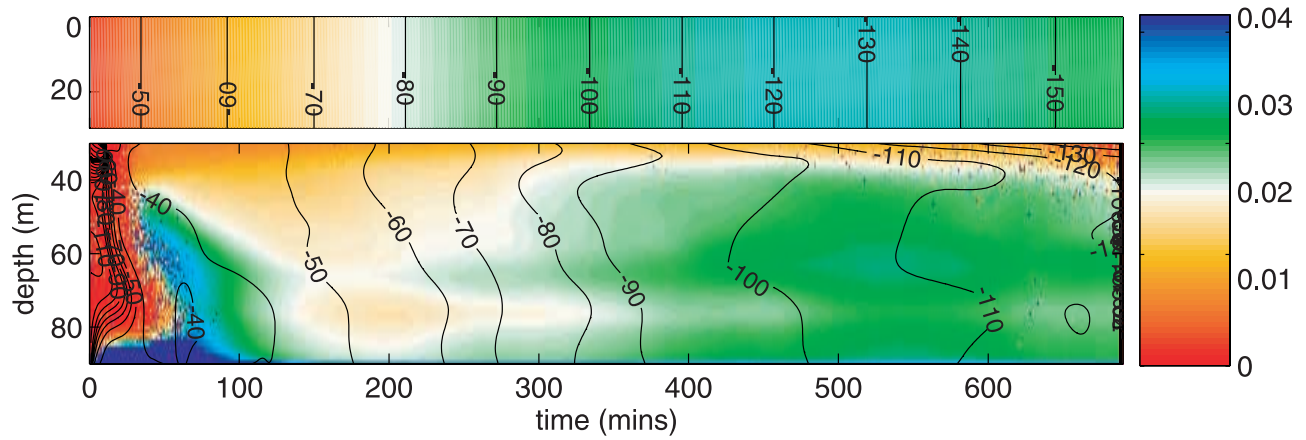

Figure 3. Plot showing phase matching between prescribed mixed-layer velocity $\boldsymbol{U_{ML}}$ (upper 30 m) and internal wave phase velocity $\boldsymbol{c_p}$ (30–90 m). The magnitudes are shaded (ms^{-1}) and the contours are corresponding horizontal vector directions (in degrees relative to the x-direction). All quantities are averaged over one hour moving windows.

mined by the domain size. The internal wave parameter values were recorded when $\boldsymbol{U_{ML}}$ had rotated a quarter cycle from the wind stress direction and the following comparisons are made between these snapshots of the independent simulations. Firstly consider the effect of halving H_0 (cf. R1 and R2). Here the horizontal wavenumber k_h remains constant since ω can not double as it is bound by N and constrained by U_{ML} (8). However, if the buoyancy frequency is also allowed to increase so that it does not constrain ω (cf. R1 and R3) then k_h does double as H_0 halves, and ω adjusts to preserve the phase speed constraint. Finally to demonstrate that k_h is not varying with N/U_{ML} we halve U_{ML}, in R4. Here, k_h remains approximately constant as ω reduces to preserve the phase velocity matching constraint.

[14] Alternatively, following the results of laboratory experiments where internal waves were generated beneath a turbulent mixed layer with a distinct vertical angle [*Dohan and Sutherland*, 2003], we conjecture that the internal waves may develop at the base of the mixed layer with properties that most rapidly flux energy out of the mixed layer. With a horizontal phase speed that is prescribed by $\boldsymbol{U_{ML}}$ this condition is satisfied when $k_z = k_h$. Computation of k_z/k_h are consistent with the hypothesis but are also very noisy.

[15] Thus the waves can be uniquely determined by the mixed-layer velocity and one of two competing mechanisms. Either there is a control on the horizontal wave number through a constraint on the Langmuir cell size, such that $k_h H_0 \approx n\pi/2$, [cf. *Wijesekera and Dillon*, 1991], subject to the additional constraint that $\boldsymbol{k_h} \cdot \boldsymbol{U_{ML}} \leq N$. Or there is a constraint that the vertical energy flux is maximized, such that $k_z = k_h$ [*Dohan and Sutherland*, 2003]. At present these simulations can not distinguish between these mechanisms as both yield internal waves with high-frequencies very near N.

[16] Downward energy and momentum fluxes from internal waves are likely to be important contributors to mixed-layer dynamics. A simple decay time-scale can be taken as the ratio of mixed-layer energy and momentum to downward fluxes of each:

$$\tau^{ke} = \frac{\int_{ML} \overline{\boldsymbol{u}^2}/2\, dz}{\overline{p'w'}(z=-H)} = 6\, days \tag{9}$$

$$\tau^{mom} = \frac{|\int_{ML} \overline{\boldsymbol{u}} dz|}{|\overline{\boldsymbol{u}'w'}|(z=-H)} = 2.5\, days, \tag{10}$$

where bar and prime terms are horizontally averaged and corresponding perturbation terms respectively. A thorough energetic analysis of the internal waves will be the subject of future work, here we simply note that these time-scales are comparable to those of energy decay from downward radiating near-inertial waves [*D'Asaro et al.*, 1995, and references therein], which are typically assumed to drain the bulk of low-frequency mixed-layer energy. Since freely propagating internal waves must have a frequency less than the local buoyancy frequency they are constrained to the highly stratified region within tens of meters from the surface mixed-layer base. Therefore, they likely deposit their energy and momentum within this transition layer, contributing to the mixing there.

4. Summary

[17] Large eddy simulation including wave processes that capture Langmuir turbulence [*Skyllingstad and Denbo*, 1995; *McWilliams et al.*, 1997; *Polton and Belcher*, 2007] of a 30 m mixed layer above a stratified region simulate the generation of internal waves. As a wind induced inertial oscillation advects the mixed layer over an uneven mixed-layer base internal waves radiate downwards. The power-weighted phase velocity is shown to match the depth averaged mixed-layer velocity. A constraint on the downward energy flux or the horizontal scale of the Langmuir cells are then sufficient to uniquely determine the high-

Table 1. Parameters From Five Simulations[a]

Run	L	H_0	U_{ML}	N	ω	k_h	$k_h H_0/\pi$
R0	225	30	0.03	4.4	3.2	0.10	1.0
R1	150	30	0.03	4.4	3.2	0.10	1.0
R2	150	15	0.03	4.4	3.8	0.12	0.6
R3	150	15	0.03	8.8	6.0	0.20	1.0
R4	150	30	0.015	4.4	2.3	0.13	1.2

[a]Units: L and H_0(m), U_{ML}(ms^{-1}), N and ω($\times 10^{-3}$ s^{-1}) and k_h(m^{-1}).

frequency, dispersive internal waves. Whilst internal waves can be generated below a wind shear driven mixed layer, that is without the inclusion of surface wave effects (not shown), inclusion of the Stokes drift processes results in a mixed layer with more deeply penetrating vertical velocities [*Polton and Belcher*, 2007] that interact with the stratified fluid. This presents exciting new grounds for the classic *Bell* [1978] mechanism that transforms energy from inertial oscillations into high-frequency internal wave energy. Since the time-scales are comparable with those for near inertial oscillations [*D'Asaro et al.*, 1995] it is estimated that under the appropriate wind and wave conditions this could be an important mechanism for draining energy out of inertial motions and into the transition layer, which is an extremely important region for mediating physical, chemical and biological interactions between surface and the deeper ocean.

[18] **Acknowledgments.** The research presented in this paper was funded by NSF, award 0525256. The authors thank the two anonymous reviewers for their constructive comments.

References

Armfield, S. W., and R. Street (2000), Fractional step methods for the Navier-Stokes equations on non-staggered grids, *ANZIAM J.*, *42*, C134–C156.

Bell, T. H. (1978), Radiation damping of inertial oscillations in the upper ocean, *J. Fluid Mech.*, *88*, 289–308.

Chini, G. P., and S. Leibovich (2005), Resonant Langmuir-circulation–internal-wave interaction. Part 2. Langmuir circulation instability, *J. Fluid Mech.*, *524*, 99–120.

Coleman, G. N. (1999), Similarity statistics from a direct numerical simulation of the neutrally stratified planetary boundary layer, *J. Atmos. Sci.*, *56*, 891–900.

Craik, A. D. D., and S. Leibovich (1976), A rational model for Langmuir circulations, *J. Fluid Mech.*, *73*, 401–426.

D'Asaro, E. A., C. C. Eriksen, M. D. Levine, P. Niiler, C. A. Paulson, and P. V. Meurs (1995), Upper-ocean inertial currents forced by a strong storm. Part I: Data and comparisons with linear theory, *J. Phys. Oceanogr.*, *25*, 2909–2936.

Dohan, K., and B. R. Sutherland (2003), Internal waves generated from a turbulent mixed region, *Phys. Fluids*, *15*, 488–498, doi:10.1063/1.1530159.

Faller, A. J. (1971), Oceanic turbulence and Langmuir circulations, *Annu. Rev. Ecol. Syst.*, *2*, 201–236.

Gargett, A. E., J. Wells, A. E. Tejada-Martinez, and G. E. Grosch (2004), Langmuir supercells: A mechanism for sediment resuspension and transport in shallow seas, *Science*, *306*, 1925–1928.

Langmuir, I. (1938), Surface motion of water induced by wind, *Science*, *87*, 119–123.

Leibovich, S. (1983), The form and dynamics of Langmuir circulations, *Annu. Rev. Fluid Mech.*, *15*, 391–427.

Lele, S. K. (1992), Compact finite difference schemes, *J. Comput. Phys.*, *103*, 16–42.

Lewis, D. M. (2005), A simple model of plankton population dynamics coupled with a LES of the surface mixed layer, *J. Theor. Bio.*, *234*, 565–591.

Li, M., and C. Garrett (1997), Mixed layer deepening due to Langmuir circulation, *J. Phys. Oceanogr.*, *27*, 121–132.

Mason, P. J., and D. J. Thompson (1992), Stochastic backscatter in large-eddy simulations of boundary layers, *J. Fluid Mech.*, *242*, 51–78.

McWilliams, J. C., P. P. Sullivan, and C.-H. Moeng (1997), Langmuir turbulence in the ocean, *J. Fluid Mech.*, *334*, 1–30.

O'Brien, M. M., A. Plueddemann, and R. A. Weller (1991), The response of oceanic mixed layer depth to physical forcing: Modelled vs. observed, *Biol. Bull.*, *181*, 360–361.

Phillips, O. M. (1977), *Dynamics of the Upper Ocean*, 336 pp., Cambridge Univ. Press, Cambridge, U. K.

Phillips, W. R. C. (2001), On an instability to Langmuir circulations and the role of Prandtl and Richardson numbers, *J. Fluid Mech.*, *442*, 335–358.

Polton, J. A., and S. E. Belcher (2007), Langmuir turbulence and deeply penetrating jets in an unstratified mixed layer, *J. Geophys. Res.*, *112*, C09020, doi:10.1029/2007JC004205.

Porté-Agel, F., C. Meneveau, and M. B. Parlange (2000), A scale-dependent dynamic model for large-eddy simulation: application to a neutral atmospheric boundary layer, *J. Fluid Mech.*, *415*, 261–284.

Rippeth, T. P., M. R. Palmer, J. H. Simpson, N. R. Fisher, and J. Sharples (2005), Thermocline mixing in summer stratified continental shelf seas, *Geophys. Res. Lett.*, *32*, L05602, doi:10.1029/2004GL022104.

Skyllingstad, E. D., and D. W. Denbo (1995), An ocean large-eddy simulation of Langmuir circulations and convection in the surface mixed layer, *J. Geophys. Res.*, *100*, 8501–8522.

Tejada-Martínez, A. E., and C. E. Grosch (2007), Langmuir turbulence in shallow water. Part 2. Large-eddy simulation, *J. Fluid Mech.*, *576*, 63–108.

Thorpe, S. A. (2004), Langmuir circulation, *Annu. Rev. Fluid Mech.*, *36*, 55–79.

Wijesekera, H. W., and T. M. Dillon (1991), Internal waves and mixing in the upper equatorial Pacific Ocean, *J. Geophys. Res.*, *96*, 7115–7125.

Zikanov, O., D. N. Slinn, and M. R. Dhanak (2003), Large-eddy simulations of the wind-induced turbulent Ekman layer, *J. Fluid Mech.*, *495*, 343–368.

J. A. Polton, Proudman Oceanographic Laboratory, 6 Brownlow Street, Liverpool L3 5DA, UK. (j.polton@pol.ac.uk)

J. A. MacKinnon and J. A. Smith, Scripps Institution of Oceanography, University of California, San Diego, 9500 Gilman Drive, La Jolla, CA 92093-0213, USA. (jmackinn@ucsd.edu; jasmith@ucsd.edu)

A. E. Tejada-Martínez, Civil and Environmental Engineering, University of South Florida, 4202 East Fowler Avenue, Tampa, FL 33620-5350, USA. (aetejada@eng.usf.edu)